Nanoscale

Accepted Manuscript

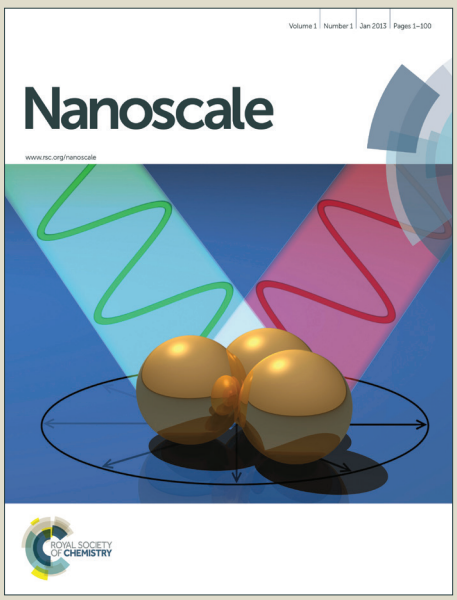

ROYAL SOCIETY OF CHEMISTRY

www.rsc.org/nanoscale

Cite this: DOI: 10.1039/c0xx00000x

www.rsc.org/xxxxxx

ARTICLE TYPE

Flexible Spiral-type Supercapacitor Based on $ZnCo_2O_4$ Nanorods Electrodes

Hao Wu,[a,b] Zheng Lou,*[,b] Hong Yang,[a] Guozhen Shen*[,b]

Received (in XXX, XXX) Xth XXXXXXXXX 20XX, Accepted Xth XXXXXXXXX 20XX

DOI: 10.1039/b000000x

Fiber electrochemical capacitors show advantages for lightweight and flexible, and may be also easily integrated or woven into various electronic devices with low cost and high efficiency. In this work, we report the preparation of $ZnCo_2O_4$ nanorods on a Ni wire as the fiber electrodes, using a simple and rapid single-step hydrothermal process. The electrochemical properties of the free-standing supercapacitor were analyzed using a two electrode system. The supercapacitor achieved a specific capacitance of 10.9 F/g. An energy density of 76 mWh/kg and a power density up to 1.9 W/kg were also obtained for the fiber supercapacitors. The flexible supercapacitor exhibited remarkable electrochemical stability when subjected to bending at various angles, illustrating the promise for use as electrodes for wearable energy storage.

1. Introduction

The increasing demands for portable and flexible electronics such as roll-up displays, photovoltaic cells, and wearable devices have initiated intensive efforts to explore flexible, lightweight and environmentally friendly energy storage devices.[1-5] As a new class of energy storage devices, flexible supercapacitors (SCs) have attracted much attention as promising energy source for wearable electronics due to their remarkable advantages such as high power density and relatively large energy density, fast charge/discharge capability, light weight, excellent reliability and flexibility. Despite the significant advances achieved in electrode materials for SCs,[6-11] the practical applications of supercapacitors were still seriously hindered due to the relatively poor performance of the electrode materials, such as low specific capacitance in carbon based materials, poor cycling stability in transition metal oxides, and very high cost of RuO_2 based materials. Therefore, more efforts are still desired to further improve the electrochemical performance of electrode materials in order to build better SCs with both high power and energy densities. It has been proven to be an effective strategy that nanostructure engineering, including nanoparticles, hollow nano-architectures and one-dimensional (1D) nanostructures could greatly contribute to the optimization of electrode properties with higher capacity/capacitance because of the increased active surface areas, short ion transport pathways and so on.[7, 12-16]

$ZnCo_2O_4$ has been considered as an attractive candidate for substitution of the conventional graphite anode in supercapacitors due to its superiorities such as improved reversible capacities, enhanced cycling stability, and good environmental benignity.[17-20] The $ZnCo_2O_4$ with a spinel structure, where the Zn^{2+} occupies the tetrahedral sites and the Co^{3+} occupies the octahedral sites, has been widely investigated as a high-performance material for supercapacitors.[17, 21, 22] In recent years, $ZnCo_2O_4$ as electrode materials for supercapacitors has begun to attract attention for its low cost and excellent electrochemical performance.[23–26] For example, Hope-Weeks's group synthesized $ZnCo_2O_4$ nanocrystals and tested its supercapacitor properties. However, the tedious preparation process and the low specific capacitance (700 F/g at 5 mV/s) made it difficult to meet the demand of practical application.[15] Liu and co-workers recently fabricated one dimensional $ZnCo_2O_4$ nanorods/nickel foam integrated electrode, although it exhibited good electrochemical performance at low current densities, its specific capacitance (1400 F/g at 1 A/g) and cycling stability (only 1000 cycles at 6 A/g were given) were still unsatisfactory.[21] Gang's group has prepared of highly porous $ZnCo_2O_4$ nanotubes, which showed a remarkable cycling ability of 689 F/g at 10 A/g after 3000 cycles together with an excellent rate capability of 588 F/g at 60 A/g (84% capacity retention).[27] From above, we can conclude that $ZnCo_2O_4$ could be considered as attractive materials.

Herein, by flexible coaxial fiber assembly of hierarchical $ZnCo_2O_4$ nanorods arrays/Ni wires electrodes, we designed a new class of flexible all-solid-state planar-integrated fiber supercapacitors (FSC), allowing us to obtain good electrochemical capacitance performance, with a high specific capacitances of 10.9 F/g at a scan rate of 10 mV/s, an energy density of 76 mWh/kg and a power density of up to 1.9 W/kg. According to our knowledge, this is the first time to grow $ZnCo_2O_4$ nanorods arrays on a Ni wire substrate and directly use it as electrode materials for supercapacitors.

2. Experimental

2.1. Synthesis of material

Hydrochloric acid (HCl), ethanol and acetone were procured from Merck (India) Ltd. Potassium hydroxide (KOH; FW=56.11),

urea($CO(NH_2)_2$; MW=60.06), Cobalt nitrate hexahydrate ($Co(NO_3)_2{\cdot}6H_2O$; FW=291.04), Ammonium fluoride(NH_4F; FW=37.04) and Zinc nitrate hexahydrate($Zn(NO_3)_2{\cdot}6H_2O$; FW=297.47) were procured from Alfa Aesar A Johnson Matthey company. Polyvinylalchol (PVA; MW=70000-100000) was procured from Himedia Laboratories Pvt. Ltd. Moreover, double distilled water was used for all the experiments.

Synthesis of the $ZnCo_2O_4$ nanorods on a Ni wire: Prior to deposition, commercial Ni wires were cleaned by sonication sequentially in acetone, 1M HCl solution, deionized water and ethanol for 15 min, respectively. After being dried, the Ni wire was transferred into Teflon-lined stainless autoclave. In a typical synthesis of $ZnCo_2O_4$ nanorods, 1 mmol $Zn(NO_3)_2{\cdot}6H_2O$, 2 mmol $Co(NO_3)_2{\cdot}6H_2O$, 6 mmol $CO(NH_2)_2$ and 5 mmol of NH_4F were dissolved in 30mL deionized water by constant stirring, and the mixture was stirred to form a pink solution in the 50 mL Teflon-lined stainless autoclave. Then, the pre-treated Ni wires was put in the above autoclave, heated to 120 ºC, and kept at that temperature for 6 h. After the autoclave cooled down to room temperature, the product was collected, washed, vacuum-dried, and then thermal treated at 350 ºC for 3 h at a rate of 5 ºC /min to obtain $ZnCo_2O_4$ nanorods.

The PVA/KOH polymer electrolyte was prepared as follows: in a typical process, 3 g PVA was dissolved in 25 mL DI water with stirring at 98 ºC for 1 h. Then, 3 g KOH was dissolved in 5 mL DI water. Finally, the above two solutions were mixed together at 60 ºC under vigorous stirring until the solution became clear.

2.2. Characterizations

The synthesized products were characterized with an X-ray diffractometer (XRD; X'Pert PRO, PANalytical B.V., the Netherlands) with radiation from a Cu target (Kα, λ=0.15406 nm). The morphologies of the samples were characterized using electron microscopy (SEM; NANOSEM 650-6700F, 15 kV) and transmission electron microscopy (HRTEM; JEOLJEM-2010HT)

2.3. Electrochemical characterization

CV examined at the scan rates of 0.01-1000 V/s and EIS recorded in the frequency range of 0.01-100 kHz with a 5 mV ac amplitude were carried out based on a CHI760D electrochemical workstation.

2.4. Calculation

The specific capacitances can be calculated from the CV curve by using the equation:[28-30]

$$C=Q/V=I/S \quad (1)$$

$$C_v=C/m \quad (2)$$

Where C is the capacitance, Q is the charge accumulated in the capacitors, V is the potential in the CV curve, I is the current in the CV curve, and S is the scan rate.[29] The energy density and power density of the device were obtained from the equations:[30]

$$E=C_{sp}\times\Delta I^2/7200 \quad (3)$$

$$P=E\times 3600/\Delta t \quad (4)$$

Where E is the energy density (in Wh/g), P is the power density (in W/g) and Δt is the total discharge time (in seconds).

3. Results and Discussions

The fabrication of the fiber solid-state SC is shown in Fig. 1. First, one commercial Ni wire sample, serving as anode, was winded around as teel rod and then pulled out, resulted in the formation of spiral-type electrode (Fig. 1 step1, 2). $ZnCo_2O_4$ nanorods grown on the Ni wire was synthesized by hydrothermal method (Fig. 1 step3), and the spiral-type electrode was then coated with a layer of PVA/KOH gel electrolyte (Fig. 1 step 4). The gel electrolyte acted not only as a separator uniformity coated on the anode and cathode wires surface but supporting materials to enable the stretch ability of the fiber device. Another $ZnCo_2O_4$ nanorods on a Ni wire sample, serving as cathode, were then inserted into the coiled, followed with the coating of more PVA/KOH electrolyte (Fig. 1 step 4). It is noticed that, if the electrolyte does not cover the whole wire surface, it will lead to short-circuit when the cathode wire was inserted into the anode one. Furthermore, the specifically selected solid-state electrolyte for the fiber SC will overcome the major drawbacks of conventional liquid electrolytes, such as leakage of electrolyte, difficulty in device integration and environmental stability, which are crucial for the development of useful wearable fiber devices.

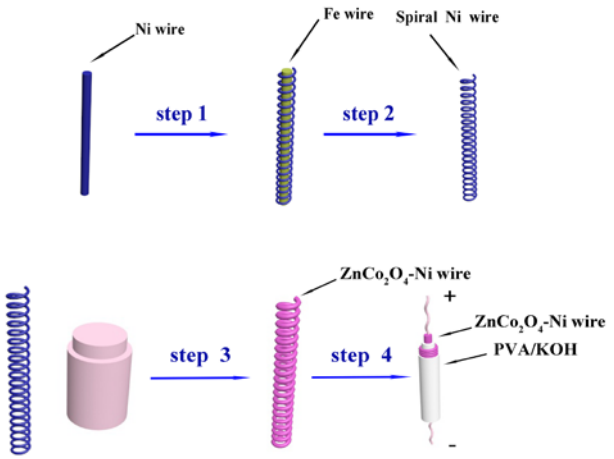

Fig. 1 Schematic illustration for designing of highly flexible coaxial fiber supercapacitors.

The $ZnCo_2O_4$ nanorods were grown on Ni wires via a conventional hydrothermal method. Fig. 2a-c shows the scanning electron microscope (SEM) images of the products with 5 mmol NH_4F. It can be seen that the $ZnCo_2O_4$ nanorods were uniformly grown on a Ni wire, as shown in Fig. 2a. Fig. 2b and c depict the SEM image of the pure $ZnCo_2O_4$ nanorods grown on Ni wires substrate with a diameter of about 50 nm. The microstructures of the $ZnCo_2O_4$ nanorods were also investigated by using transmission electron microscopy (TEM). Fig. 2d shows a low-magnification TEM image of single $ZnCo_2O_4$ nanorods. From the image we can see that the $ZnCo_2O_4$ nanorods have a porous structure with a diameter of about 50 nm which agree well with the SEM images. One-dimensional nanorods could greatly contribute the higher capacity/capacitance because of the increased active surface areas, short ion transport pathway. Fig. 2e demonstrates the HRTEM image of a single porous $ZnCo_2O_4$ nanorod. The clearly resolved lattice fringes show that the d-spacing of 0.24 and 0.28 nm marked in the pattern could be indexed to the (311) and (220) crystal planes of $ZnCo_2O_4$ phase, which further confirmed the formation of crystalline $ZnCo_2O_4$

nanorods and agreed well with the result of X-ray diffraction (XRD) data.[31] The phase and composition of the nanorods were investigated by peeling off the nickel wires. As shown in Fig. 2f, the XRD pattern of the precursor is well consistent with previous reports.[32-34] It is obvious that all of the observed peaks position are in good agreement with the $ZnCo_2O_4$ structure of standard card of JCPDS card no. 23-1390.

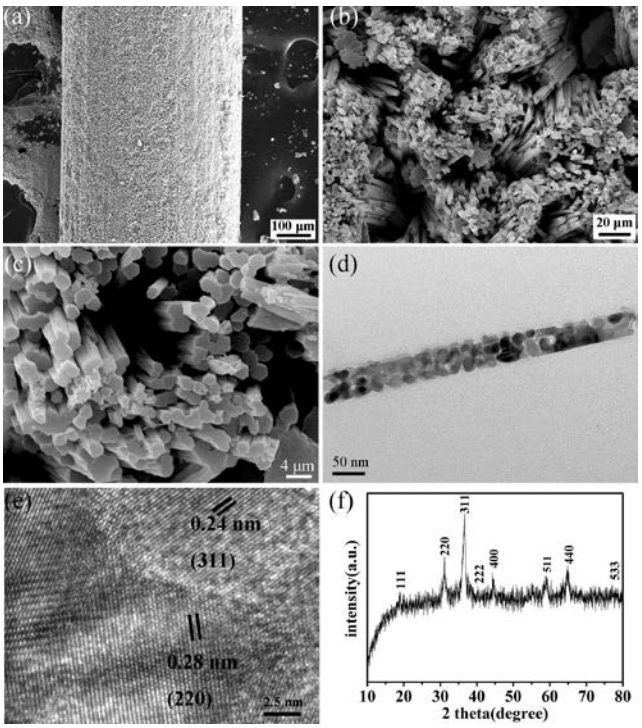

Fig. 2 (a,b,c) SEM images of $ZnCo_2O_4$ nanostructures grown on Ni wires, (d) TEM and (e) HRTEM image; (f) XRD pattern of the as-obtained $ZnCo_2O_4$ nanorods.

The electrochemical properties of the $ZnCo_2O_4$ nanorods on a Ni wire electrode were first measured in a three-electrode cell using 3 M KOH electrolyte, a platinum electrode. And a saturated calomel electrode (SCE) were used as the counter electrode and reference electrode, respectively. Fig. 3a shows the representative cyclic voltammetry (CV) curves recorded at different scan rates ranging from 10 to 100 mV/s, and one pair of redox peaks can be clearly seen. All of the curves show obvious pseudocapacitance features with a pair of well-defined redox peaks within 0-0.45 V (vs. SEC). The pair of peaks is mainly associated with the Faradaic redox reaction related to M–O/M–O–OH, where M refers to Ni or Co.[32, 33] Accompanying the increase in the scan rate, the peak currents were also increased, suggesting that the one-dimensional porous nanorods were beneficial to fast redox reactions, furthermore no redox peaks can be observed in the pure nickel wire at 10 mV/s. To further evaluate the potential application of the $ZnCo_2O_4$ as electrodes for electrochemical supercapacitors, galvanostatic charge–discharge measurements were carried out between 0 and 0.45 V (vs. SEC) at various current ranging from 0.8 to 3.0 mA, as shown in Fig. 3b. The voltage plateaus during the charge/discharge process were consistent with the CV results and the nonlinear characteristics further verified the pseudocapacitance behavior. The electrochemical reaction of $ZnCo_2O_4$ with the electrolyte can be written as follows:

$$ZnCo_2O_4+OH^- \rightarrow ZnCo_2O_4/OH+ ZnCo_2O_4\text{-}OH$$

Here, $ZnCo_2O_4/OH$ represents the electric double layer formed by the hydroxyl ion, and $ZnCo_2O_4$-OH represents the product formed by the cathode reaction involving the hydroxyl ion.[35]

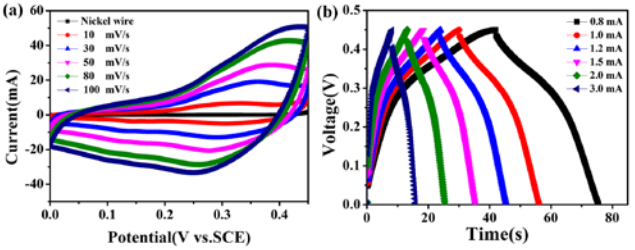

Fig. 3 (a) CV curves of the $ZnCo_2O_4$ nanorods /nickel wire at the different scan rates; (b) The galvanostatic Charge/discharge curves at different currents.

Fig. 4a shows a galvanostatic charging–discharging test which was conducted in a stable potential window between 0 and 1 V at various current densities ranging from 0.5 to 2 mA. We can observe that the charge/discharge behavior has a good symmetry, indicating the charge/discharge straight line was provided with excellent coulomb efficiency.[36] Fig. 4b illustrates the charge/discharge behavior of the FSC devices at a current of 0.5 mA. A relatively small voltage drop (0.15 V) was shown in Fig. 4b, indicating excellent SC performance of the as-designed FSC. From Fig. 4c, we can judge that the FSC devices are operated by scan rates ranging from 10 to 200 mV/s. From the plot, it can be observed that the curves of the two electrode systems are obviously different with those of the above three-electrode systems (Fig. 3a), which mainly represent the absence of redox peaks. Briefly, supercapacitors can be classified into two categories: the non-Faradic electrical double-layer capacitor and Faradaic redox pseudocapacitor. These two mechanisms can work separately or together, depending on the active electrode materials used in the capacitors. For our two-electrode system, it clearly reveals that the feature of electrical double-layer capacitor occupied dominant position than that of typical pseudocapacitor. Besides, no obvious redox peaks are observed in the present work, indicating that the current supercapacitors are charged and discharged at a pseudoconstant rate.[37, 38] Thus, we can get the conclusion that the two-electrode devices are primarily nonfaradaic within their corresponding voltage window.[27] Actually, this common phenomenon is observed in many symmetric supercapacitors reported previously.[26] We calculated the capacity of the flexible device at different scan rate, ranging from 10 to 100 mV/s and the corresponding result was depicted in Fig. 4d. From the curve, the largest capacitance could be obtained to be about 10.90 F/g at a scan rate of 10 mV/s, and the specific capacitance was calculated to range from 4.85 F/g at 100 mV/s to 10.90 F/g at 10 mV/s, which was higher than that of $ZnCo_2O_4$@carbon fibers (0.4 mF at 100 mV/s to 0.85 mF at 30 mV/s)[26] and revealed that one-dimensional $ZnCo_2O_4$ nanorods could greatly contribute to the optimization of electrode properties with higher capacity/capacitance. The cycling performance of the FSC at progressively increased current was

carried out as shown in Fig. 4e. After 800 times of continuous cycling at varied current, the current returned to 1 mA and obtained to be 97.9% of the initial capacitance at 1 mA. And then it can be recovered and maintained for another 200 cycles, which was much higher than previous reported values.[21, 30] Fig. 4f shows the cyclic stability, we can find that the capacitance maintained at 92% of its original value at 2 mA after 3500 charge/discharge cycles, revealing its excellent cycling stability, which can be attributed to the mechanical stability of the active materials and good contact between the electrode and current collector origin to the direct growth of $ZnCo_2O_4$ nanostructures on the Ni wire substrate. Above that, it makes possible to consider as an attractive candidate in supercapacitors due to its superiorities such as improved reversible capacities, enhanced cycling stability.

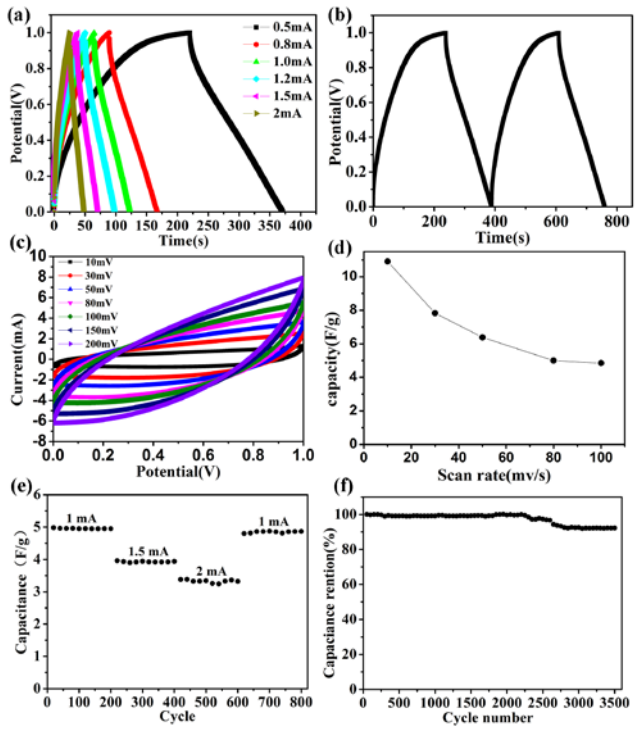

Fig. 4 (a) Galvanostatic charge–discharge at different currents measured in the voltage window of 0-1 V; (b) Galvanostatic charge/discharge curve at a current of 0.08 mA; (c) Cyclic voltammograms from 10 to 200 mV/s; (d) The plot of the capacitance as a function of potential at various scan rates; (e) Cycle performance with the increasing currents; (f) Capacitance retention on cycle number at a current of 2 mA.

Electrochemical impedance spectroscopy (EIS) and rate capability are two important parameters to determine the performances of SCs. Fig. 5a shows the energy density and power density (Ragone chart). The energy density varied from 42 to 76 mWh/kg in a power density ranging from 0.50 to 1.9 W/kg. Our fabricated FSC also revealed an open circuit voltage of 0.4 V which can be maintained for 10.8 h after fully charged and also have a low leakage current of 0.4 mA (Fig. 5b and c), indicating the excellent energy storage performance. Fig. 5d and inset show the Nyquist plots in the frequency ranging from 100 kHz to 0.01 Hz with an acperturbation of 5 mV. In the high frequency region, the intercept of the semicircle with the real axis represents the equivalent series resistance (ESR) including the resistance of the electrolyte solution, the intrinsic resistance of the active material, and the contact resistance of the interface active material/current collector. The x-intercept of the Nyquist plots represent the ESR of two-electrode SC and the charge transport resistance is 2.23 Ω, [39] revealing that our electrodes have a very small resistance with good ion response. The reason may be that one-dimensional nanorods could short ion transport pathway and decrease resistance.

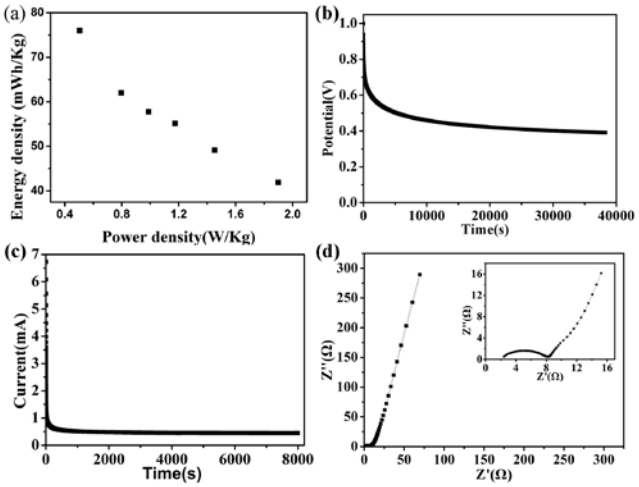

Fig. 5 (a) Volume energy and power density of the fiber solid-state supercapacitor; (b) Self-discharge curve and (c) Leakage current curve of the device; (d) Nyquist plots showing the imaginary part versus the real part of impedance. Inset shows the high-frequency region of the plot.

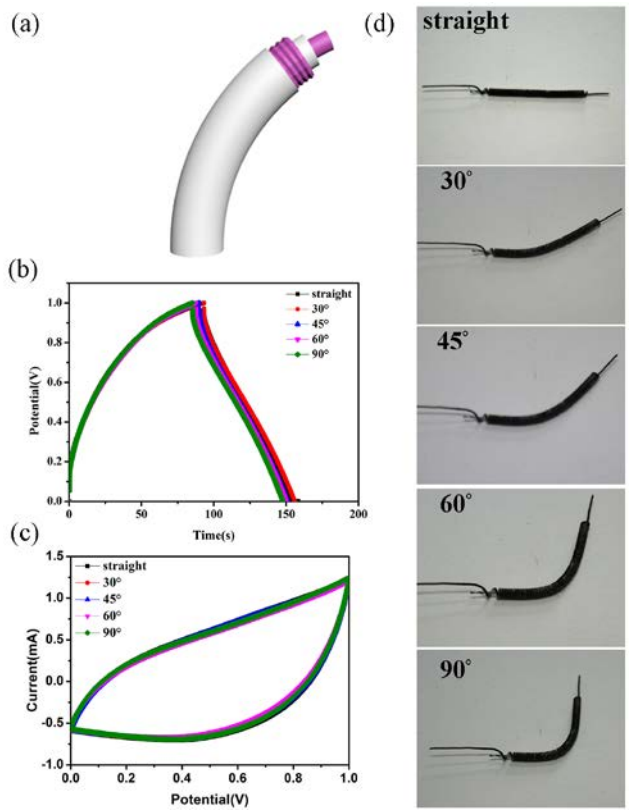

Fig. 6 (a) Fiber SCs in bending states; (b) Charge/discharge curves at a current of 1.5mA in straight and different bending states, respectively;

(c) CV curves at 100 mV/s in straight and different bending states, respectively; (d) Photos of coaxial FSC under the different bending states, straight, 30º, 45º, 60º, 90º.

Mechanical stability of the FSC under bending states is a key parameter for practical using. Compared with the planar device, the fiber device can be strong enough to bear the generated tensile force and the performance of fiber supercapacitors is almost same under the different angles, which is very useful in practical applications.[40] Thus the flexibility of our coaxial FSC was further performed. Fig. 6a Schematic diagram shows the FSCs in different bending states. Fig. 6b shows the charge/discharge curves at a current of 1.5 mA under the different angles, which demonstrate our device can maintain good fiber shape and have an excellent flexibility. Fig. 6c demonstrates the CV curves of the FSC deformed from the straight state to the 90º status. Meanwhile the little performance degradation indicates the high stability of the as-fabricated coaxial FSC. Fig. 6d presents the photos of our coaxial FSC under the different bending states (30º, 45º, 60º, 90º), which demonstrated our device has an excellent flexibility. These results make it possible to design patterns for wearable devices applications.

4. Conclusions

We have successfully developed a spiral-type flexible fiber supercapacitor based on $ZnCo_2O_4$ nanorods electrodes as active materials on a Ni wire. The specific capacitances reached 10.9 F/g at a scan rate of 30 mV/s, an energy density of 76 mWh/kg and a power density of up to 1.9 W/kg. The outstanding cycle ability and excellent flexibility have also been achieved. The enhanced performance is attributed to one-dimensional $ZnCo_2O_4$ nanorods structural which increasing active surface areas, shorting ion transport pathways and so on. In view of the excellent electrochemical performance and the facile and cost-effective synthesis, these $ZnCo_2O_4$ nanostructures might hold great promise as advanced electrode materials for high-performance supercapacitors. Furthermore, by decreasing the diameter of the metal fiber, flexible fiber supercapacitors with smaller diameter and size are expected to be fabricated, which will make it possible to weave the fiber supercapacitor in to design patterns for wearable electronics applications.

Acknowledgements

This work was supported by the National Natural Science Foundation (61377033).

Notes and references

[a] *The Key Laboratory of Resource Chemistry of Ministry of Education, Shanghai Key Laboratory of Rare Earth Functional Materials, and Shanghai Municipal Education Committee Key Laboratory of Molecular Imaging Probes and Sensors, Shanghai Normal University, Shanghai 200234, China.*

[b] *State Key Laboratory for Superlattices and Microstructures, Institute of Semiconductors, Chinese Academy of Sciences, Beijing 100083, China. E-mail: zlou@semi.ac.cn; gzshen@semi.ac.cn.*

1. M. F. El-Kady and R. B. Kaner, *Science*, 2012, **335**, 1326.
2. G. H. Yu and Y. Cui, *Nano Energy*, 2013, **2**, 213.
3. X. Lu, Y. Zeng, M. Yu, T. Zhai, C. Liang, S. Xie, M. Balogun and Y. X. Tong, *Adv. Mater*., 2014, **26**, 3148.
4. B. Yao, L. Y. Yuan, X. Xiao, J. Zhang , B. Hu and W. Chen, *Nano Energy*, 2013, **2**, 1071.
5. N. Liu, W. Ma, J. Tao, X. Zhang, J. Su, L. Li, C. Yang, D. Golberg and Y. Bando, *Adv. Mater*.,2013, **25**, 4925.
6. P. J. Hall, M. Mirzaeian, S. I. Fletcher and F. B. Sillars, *Energy Environ. Sci*., 2010, **3**, 1238.
7. A. S. Arico`, S. A. Antonino, P. Bruce, B. Scrosati, J. M. Tarascon and W.V. Schalkwijk, *Nat. Mater*., 2005, **4**, 366.
8. Z. G. Yin and Q. D. Zheng, Adv. *Energy Mater*., 2012, **2**, 179.
9. Y. Fang, B. Luo, Y. Y. Jia, X. L. Li, B. Wang, Q. Song and F. Y. Kang, *Adv. Mater*., 2012, **24**, 6348.
10. L. Zhang, W. Bin and H. X. W. Lou, *Chem. Commun*., 2012, **48**, 6912.
11. T. Zhu, J. S Chen and X. W. Lou, *J. Mater. Chem*., 2010, **20**, 7015.
12. L. L. Wnag, J. N. Deng, Z. Lou and T. Zhang, *J. Mater. Chem. A*, 2014, **2**, 10022.
13. X. W. Lou, L. A. Archer and Z. C. Yang, *Adv. Mater*., 2008, **20**, 3987.
14. L. L. Wang, H. M. Dou, Z. Lou and T. Zhang, *Nanoscale*, 2013, **5**, 2686.
15. M. Davis, C. Guemeci, B. Black, C. Korzeniewski and L. Hope Weeks, *RSC Adv*., 2012, **2**, 2061.
16. L. L. Wang, T. Fei, Z. Lou and T. Zhang, *ACS Appl. Mater. Interfaces*, 2011, **3**, 4689.
17. Y. Sharma, N. Sharma, G. Rao and B. Chowdari, *Adv. Funct. Mater*., 2007, **17**, 2855.
18. Y. C. Qiu, S. H. Yang, H. Deng and L. M. Jin, *J. Mater. Chem.*, 2010, **20**, 4439.
19. N. Du, Y. F. Xu, H. Zhang, J. X. Yu, C. X. Zhai and D. R. Yang, *Inorg. Chem.*, 2011, **50**, 3320.
20. D. Deng and J. Y. Lee, *Nanotechnology*, 2011, **22**, 355.
21. B. Liu, B. Y. Liu and G. Z. Shen, *ACS Appl. Mater. Interfaces*, 2013, **5**, 10011.
22. Y. C. Qiu, S. H. Yang, H. Deng and W. S. Li, *J. Mater. Chem.*, 2010, **20**, 4439.
23. W. Luo, X. L. Hu, Y. M. Sun and Y. H. Huang, *J. Mater. Chem.*, 2012, **22**, 8916.
24. K. Karthikeyan, D. Kalpana and N. G. Renganathan, *Ionics*, 2009, **15**, 107.
25. M. Davis, C. Guemeci and B. Black, *RSC Adv*., 2012, **2**, 2061.
26. B. Liu, D. S. Tan, X. F. Wang, D. Chen and G. Z. Shen, *Small*, 2013, **9**, 1998.
27. G. Zhou, J. Zhu, Y. J. Chen and T. H. Wang, *Electrochimica. Acta*, 2014, **123**, 450.
28. G. Pandolfo and A. F. Hollenkamp, *Journal of Power Sources*, 2006, **157**, 11.
29. J. Bae, M. K. Song, Y. J. Park, J. M. Kim, M. L. Liu and Z. L. Wang, *Angew. Chem. Int. Ed*., 2011, **50**, 1683.
30. Q. F. Wang, X. F. Wang and G. Z. Shen, *Nano Energy*, 2014, **8**, 44.
31. F. X .Bao, X. F Wang and X. Y. Liu, *RSC Adv*., 2014, **4**, 2393.
32. H. L. Wang, Q. M. Gao and L. Jiang, *Small*, 2011, **7**, 2454.
33. S. V. Bangale and R. D. Prakshale, *J Porous Mat.*, 2012, **2**, 20.
34. B. Liu, J. Zhang, X. F. Wang, G. Chen, D. Chen, C. W. Zhou and G. Z. Shen, *Nano Lett.*, 2012, **12**, 3005.
35. D. Choi, G. E. Blomgren and P. N. Kumta, *Adv.Mater*., 2006, **18**, 1178.
36. M. D. Stoller and R. S. Ruoff, *Energy Environ. Sci.*, 2010, **3**, 1294.
37. L. Yang, S. Cheng, Y. Ding, X. B. Zhu, Z. L, Wang and M. L. Liu, *Nano Lett.*, 2012, **12**, 321.
38. X. Y. Lang, A. Hirata, J. T. Fu and M. W. Nat. Chen, *Nanotechnol.*, 2011, **6**, 232.
39. D. W. Wang, F. Li, W. C. Ren, Z. G. Chen, J. Tan, Z.S. Wu, I. Gentle, G. Q. Lu and H. M. Cheng, *ACS Nano*., 2009, **3**, 1745.
40. H. Sun, X. You, J. Deng and H. S. Peng, *Angew. Chem. Int. Ed.*, 2014, **53**, 6664.